Rapid Communications

Electrically switchable Rashba-type Dzyaloshinskii-Moriya interaction and skyrmion in two-dimensional magnetoelectric multiferroics

Jinghua Liang,[1] Qirui Cui,[1] and Hongxin Yang[1,2,*]

[1]*Ningbo Institute of Materials Technology and Engineering, Chinese Academy of Sciences, Ningbo 315201, China*

[2]*Center of Materials Science and Optoelectronics Engineering, University of Chinese Academy of Sciences, Beijing 100049, China*

(Received 5 July 2020; revised 10 October 2020; accepted 7 December 2020; published 22 December 2020)

Realizing topological magnetism and its electric control are intensive topics in spintronics due to their promising applications in information storage and logic technologies. Here, we unveil that both can be achieved in two-dimensional (2D) magnetoelectric multiferroics. Using first-principles calculations, we show that a strong Dzyaloshinskii-Moriya interaction (DMI), which is the key ingredient for the formation of exotic chiral magnetism, could be induced in 2D multiferroics with vertical electric polarization via the Rashba effect. We verify that such a significant DMI can promote the stabilization of sub-10-nm skyrmions in 2D multiferroics with perpendicular magnetic anisotropy such as a CrN monolayer. In addition, the presence of both magnetization and electric polarization in 2D multiferroics provides us with the unique opportunity for the effective electric control of both the strength and chirality of the DMI and thereby the topological magnetism. As an example, we introduce four multiferroic skyrmions with different chiralities and polarities that can be manipulated by an external field.

DOI: 10.1103/PhysRevB.102.220409

Introduction. Topological chiral spin textures, e.g., spin spirals [1,2] and skyrmions [3–5], are of particular interest from both fundamental and applied points of view. A crucial ingredient for the generation of exotic topological magnetism is the antisymmetric Dzyaloshinskii-Moriya interaction (DMI) [6,7] that results from spin-orbit coupling (SOC) in magnets with inversion asymmetry, favoring noncollinear spin configurations. The induction and control of the DMI are essential steps towards spintronics applications of topological magnetism.

In the last decade, much research has been devoted to employ ferromagnet/heavy metal (FM/HM) heterostructures, such as Fe/Ir [8], PdFe/Ir [9], and Co/Pt [10], with a strong interfacial DMI to realize skyrmions. Recently, with the breakthrough in experimental realizations [11–15], two-dimensional (2D) intrinsic ferromagnetic thin films, such as CrI_3 [12], VSe_2 [13], and Fe_3GeTe_2 [15] monolayers, have attracted a lot of interest. However, the absence of a DMI in the former 2D magnets due to a symmetry constraint has hindered their application in skyrmion-based spintronics. In a very recent work [16], we find that 2D magnets with a Janus structure can acquire a very large DMI through the Fert-Levy mechanism as for FM/HM heterostructures, in which heavy nonmagnetic atoms act as SOC-active sites for electron hopping, yet it is unclear whether a strong DMI can be induced in 2D materials via other mechanisms. We note that 2D magnetoelectric multiferroics with vertical electric polarization (hereafter referred to as 2D multiferroics unless stated otherwise) may be excellent candidates for the realization of a Rashba effect induced DMI [17–19], since their structure inversion symmetry is naturally broken and intrinsic Rashba SOC additionally exists due to the electrostatic potential difference generated by the vertical electric dipole. Comparing to the Fert-Levy mechanism, a Rashba-type DMI has the advantage that it does not necessarily require heavy atoms to provide strong SOC, which is a benefit to achieve low Gilbert damping for efficient magnetization switching [20]. In addition, with the coexistence of magnetization and electric polarization in these multiferroics, both the strength and chirality of the DMI and thereby the topological magnetism could be effectively controlled by an electric field.

In this Rapid Communication, we perform first-principles calculations and micromagnetic simulations to demonstrate that 2D multiferroics, such as the recently predicted monolayers of CrN [21], $CuMP_2X_6$ (M = Cr, V; X = S, Se) [22], and vacancy-doped CrI_3 (Cr_8I_{23}, i.e., 2 × 2 CrI_3 supercell with one I vacancy) [23], naturally host Rashba-type DMI that can facilitate the emergence of topological magnetism. Furthermore, we show how the induced DMI and skyrmion can be controlled by an electric field. The subject of a skyrmion and its electric control in multiferroics has been extensively discussed for bulk [24,25] and heterostructured [26] materials, but still needs to be addressed for 2D multiferroics.

Proposal for electric control of the DMI and topological magnetism in 2D multiferroics. We note that the two stable states with opposite spontaneous polarizations **P** in a double-well energy landscape can be switched by an out-of-plane electric field [see Fig. 1(a)]. Concurrently, the chirality of their associated DMI is also reversed since those two states are connected by a horizontal reflection operation. Importantly, this mechanism can be utilized to manipulate topological magnetic structures such as skyrmions. A skyrmion has degrees of

*Author to whom correspondence should be addressed: hongxin.yang@nimte.ac.cn

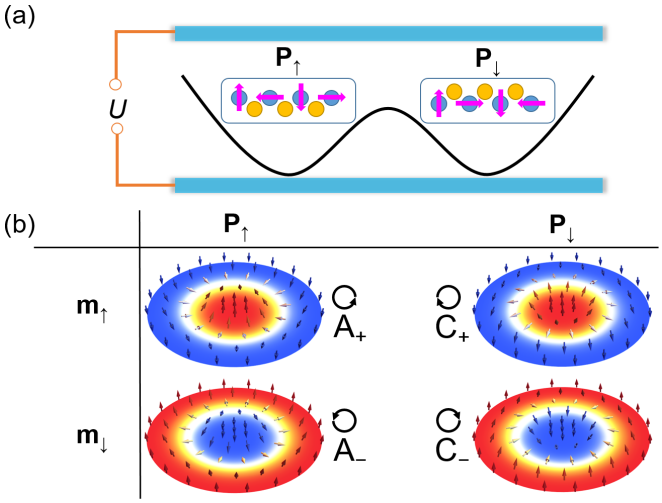

FIG. 1. Concept of the switchable DMI and multiferroic skyrmions. (a) With the electric field switching of polarization **P** for the two stable states in the double-well energy landscape of 2D multiferroics, the chirality (indicated by the magenta arrows) of their associated DMI is also reversed. (b) The four interswitchable multiferroic skyrmions with different chiralities and polarities, which can be distinguished by the notations A_+, A_-, C_+, and C_- as well as the corresponding icons of the rotating circular arrow.

freedom of chirality that indicates the spin swirling direction and is imposed by the chirality of the DMI, which in turn is determined by the direction of **P**, and polarity that specifies the direction of magnetization **m** in the skyrmion core [27], which can be transformed by a magnetic field [28,29]. With the different combinations of directions of **P** and **m**, we can realize four degenerate interswitchable skyrmionic states with different chiralities and polarities in a single 2D multiferroics as schematically shown in Fig. 1(b). We have introduced the notations A_+, A_-, C_+, and C_- as well as the corresponding icons of a rotating circular arrow to distinguish the four skyrmions, where the characters A and C correspond to anticlockwise and clockwise chirality and the subscripts "+" and "−" indicate an upward and downward polarity, respectively. To switch between the four degenerated skyrmions, one can first apply a magnetic field to fix the polarity and then the electric field to control the chirality. The manipulation of interswitchable multiferroic skyrmions can inspire another concept in the design of high-density skyrmion-based memory and logic devices. In the following, we first take a CrN monolayer as a representative example to demonstrate the existence of Rashba-type DMI and skyrmions as well as their electric control, and then extend the discussions to other thin films.

Methodology. The micromagnetic energy functional of a spin spiral for a thin film reads [30]

$$E[q] = Aq^2 + Dq - \frac{K}{2}, \tag{1}$$

where q is the spiral length, A is the exchange stiffness, D is the DMI parameter, and $K = K_u - M_s\mu_0^2/2$ is the effective anisotropy corrected by the demagnetization effect with K_u being the magnetocrystalline anisotropy, M_s the saturation magnetization, and μ_0 the vacuum permeability. Here, we adopt the sign convention that $D > 0$ ($D < 0$) implies an anticlockwise (clockwise) DMI, and $K > 0$ ($K < 0$) indicates perpendicular (in-plane) anisotropy. It is convenient to introduce the dimensionless parameter

$$\kappa = \left(\frac{4}{\pi}\right)^2 \frac{AK}{D^2}. \tag{2}$$

For $\kappa < 1$, the magnetic structure of the system exhibits spin spirals as the ground state, whereas for $\kappa > 1$, an isolated metastable skyrmion could be formed in the background of a ferromagnetic ground state [31–33]. We have implemented the qSO method [34], which treats the SOC within the first-order perturbation theory and in a self-consistent way for the calculation of $E[q]$ in Eq. (1), in conjunction with the VASP package [35] to determine the magnetic parameters (see the Supplemental Material [30] for details and Refs. [34–39] therein).

Rashba-type DMI in a CrN monolayer. A CrN monolayer with a hexagonal structure [see the top and side views of the structure in Figs. 2(a) and 2(b)] is a recently predicted 2D metallic multiferroics [21]. The relaxed CrN monolayer has a lattice constant a of 3.16 Å and a small buckling distance h of 0.21 Å, which results in an out-of-plane electric polarization of 6.68 pC/m [indicated by the green arrow in Fig. 2(b)]. Consistent with previous research [21,40], our calculations show that the buckled ferroelectric CrN monolayer has a lower energy of 9.08 meV/f.u. than the planar paraelectric one, which indicates that spin-phonon coupling is responsible for its vertical ferroelectricity.

The structure inversion asymmetry induced by vertical ferroelectric displacement could lead to a DMI between Cr atoms. To demonstrate such an effect, we calculate $E[q]$ in the interval of $|q| \leqslant 0.1\frac{2\pi}{a}$ [see Fig. 2(c)]. Clearly, we can see that when SOC is neglected [black points in the upper part of Fig. 2(c)], spin spirals with q and $-q$ are degenerate, and the ground state is the ferromagnetic state ($q = 0$). Once SOC is included, as expected, $E[q]$ [red points in the upper part of Fig. 2(c)] becomes asymmetric, where the anticlockwise rotating spin spiral [see the inset in Fig. 4(b) for an illustration of spin chirality] is more favorable, due to the effect of the DMI. From the zoom-in plot of $E[q]$ around $q = 0$ [see the inset in the upper part of Fig. 2(c)], we can find that the lowest $E[q]$ locates at $q = -0.006\frac{2\pi}{a}$, corresponding to a spiral period length of $\lambda = \frac{2\pi}{|q|} = 52.67$ nm. With the calculated DMI energy $\Delta E_{\mathrm{DM}}[q] = (E[q] - E[-q])/2$ [see the lower part of Fig. 2(c)], which shows good linear dependence on q, D and A can be determined to be 3.74 meV Å/f.u. and 142.89 meV Å^2/f.u., respectively. Here, the positive sign of D indicates that the CrN monolayer prefers an anticlockwise DMI when its polarization **P** points along the $+z$ direction. The calculated K_u is 0.22 meV/f.u. and M_s is 2.40 μ_B/f.u. Then we can deduce that κ is only 1.68, which is near the critical value ($\kappa = 1$) for the transition to a spiral state so that an isolated metastable skyrmion can be stabilized in the CrN monolayer. We will return to this point later.

Next, we explore the microscopic origin of DMI in a CrN monolayer. It is helpful to use the atom-resolved $\Delta E_{\mathrm{DM}}[q]$ to examine the energy source of the DMI [34,41], as shown in Fig. 3(a) for $q = -0.006\frac{2\pi}{a}$. One can clearly see that ΔE_{DM} is dominated by Cr atoms and has a negligible contribution

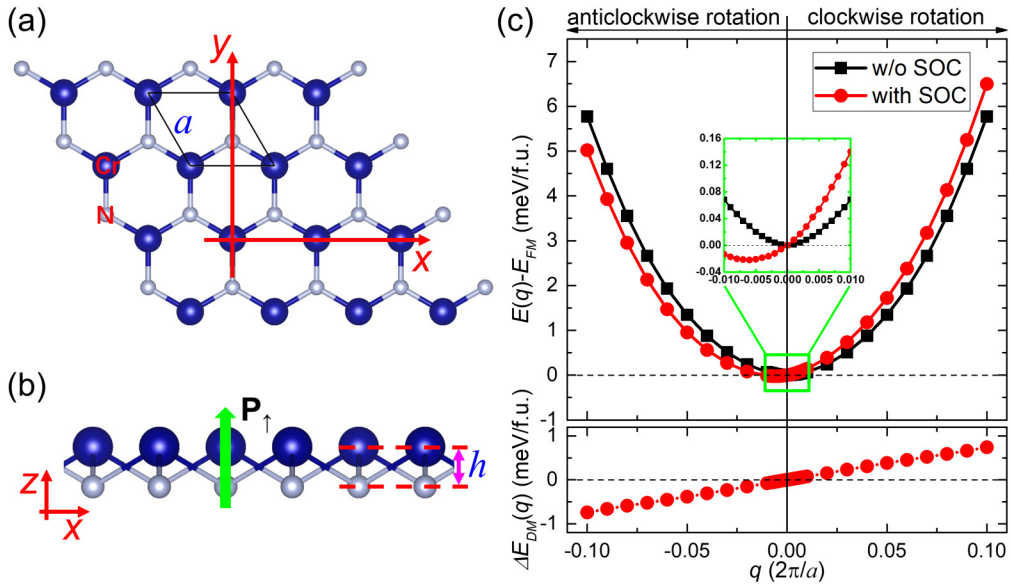

FIG. 2. (a) Top and (b) side views of the crystal structure of a CrN monolayer with a lattice constant a and buckling distance h. (c) Spin spiral energy $E[q]$ (upper panel) and DMI energy $\Delta E_{\mathrm{DM}}[q]$ (lower panel) calculated as a function of spiral vector length q. $E[q]$ is given with respect to the ferromagnetic state at $q = 0$. Black and red points are calculated without (w/o) and with SOC, respectively.

from N atoms. This feature is in great contrast to that in FM/HM multilayers [41,42] and our previously studied 2D Janus manganese dichalcogenides [16], whose DMI energy is contributed mostly by the heavy nonmagnetic atoms, which is typical for the DMI generated via the Fert-Levy mechanism. However, we can identify that it is representative for the Rashba-type DMI as in graphene/Co heterostructures [43]. To confirm that the DMI is mediated by the conduction electrons with Rashba SOC, we plot the electronic band structures of a CrN monolayer with magnetization pointing along the $[1\bar{1}0]$ and $[\bar{1}10]$ directions [see Fig. 3(b)], which show characteristic Rashba-type $\boldsymbol{k}$ -dependent splitting. For a Rashba-type DMI, the DMI parameter can be estimated as $D_R = (\frac{4m^*\alpha_R}{\hbar^2})A$ [17], where $\hbar$ is the reduced Planck constant, m^* is the effective mass of the electron, α_R is the Rashba coefficient, and $A = 142.89\,\mathrm{meV\,\AA^2/f.u.}$ is the calculated spin stiffness. Here, we

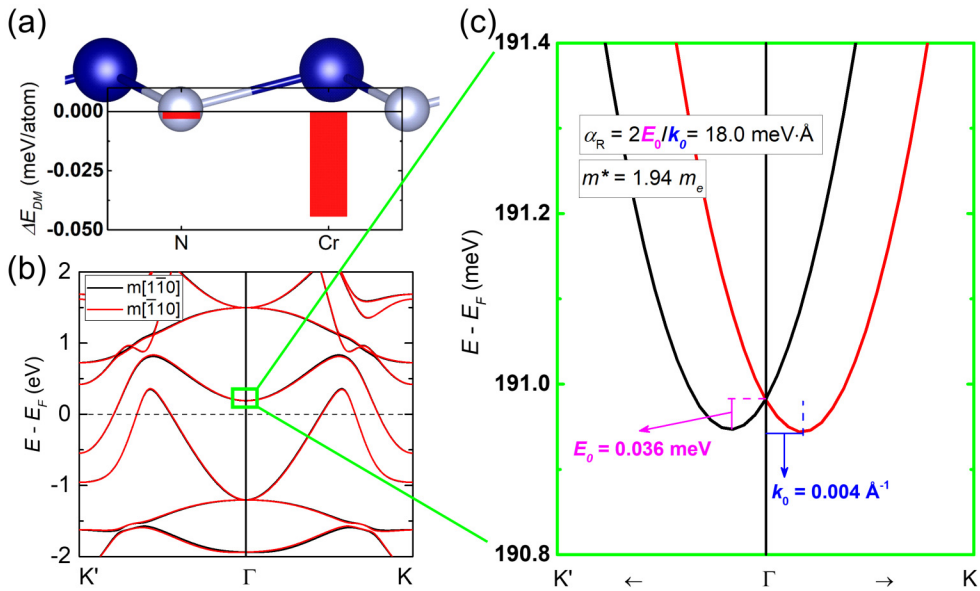

FIG. 3. (a) Atom-resolved DMI energy $\Delta E_{\mathrm{DM}}[q]$ at $q = -0.006\frac{2\pi}{a}$, where the minimum of $E[q]$ locates. (b) Band structures of a CrN monolayer with magnetization with the magnetization direction along $[1\bar{1}0]$ (black lines) and $[\bar{1}10]$ (red lines). (c) Zoom-in plot of band structures for states that are around the Γ point and close to the Fermi level. For these states, we can extract that the effective mass $m^* = 1.94m_e$ and the Rashba coefficient $\alpha_R = 2E_0/k_0 = 18.0\,\mathrm{meV\,\AA}$ with E_0 being the Rashba splitting at the wave vector k_0.

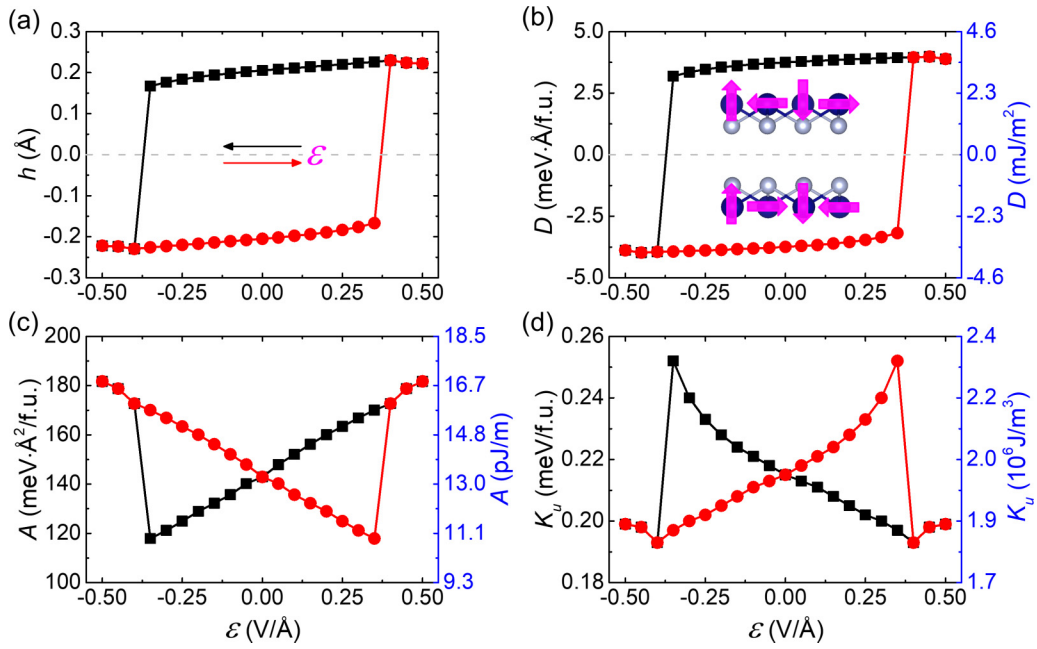

FIG. 4. The calculated (a) buckling distance h, (b) DMI parameter D, (c) spin stiffness A, and (d) magnetocrystalline anisotropy K_u as the out-of-plane electric field ε sweeps from 0.50 to -0.50 V/Å (black points), and vice versa (red points). The blue right axes in (b) and (c) indicate the values of magnetic parameters with converted units [44]. The inset in (b) presents the preferred chirality (indicated by the magenta arrows) of the spin spiral for an anticlockwise ($D > 0$) and clockwise ($D < 0$) DMI.

focus on the electronic states that are around the Γ point and close to the Fermi level. From the zoom-in plot in Fig. 3(c), $\alpha_R = 18.0$ meV Å and $m^* = 1.94\, m_e$, with m_e being the rest mass of the electron that can be extracted. One can then deduce that $D_R = 2.66$ meV Å/f.u., which is only slightly smaller than our previous value ($D = 3.74$ meV Å/f.u.) calculated by the qSO method. Altogether, we can infer that the DMI in a CrN monolayer originates from the Rashba effect.

Electric control of magnetic parameters in a CrN monolayer. Here, we show that both the structural and magnetic properties of a CrN monolayer can be effectively controlled by an out-of-plane electric field. Figure 4(a) presents the variation of buckling distance h when the electric field ε sweeps from 0.50 to -0.50 V/Å (black points), and vice versa (red points). From the hysteresis loop of h, we can see that as ε changes from 0.50 to -0.50 V/Å, h first increases slightly when $\varepsilon \geqslant 0.40$ V/Å, then decreases monotonously from 0.23 to 0.17 Å before the electric polarization switching occurs at about $\varepsilon = -0.40$ V/Å. The variation of h reflects the electric field control of ferroelectric displacement.

Figures 4(b)–4(d) summarize the resulting electric-field-dependent magnetic parameters [44]. Notably, from Fig. 4(b), we can see that the variation trend of D almost follows that of h. Within the range of $|\varepsilon| < 0.50$ V/Å, the absolute value of D can be tuned between 3.98 and 3.19 meV Å/f.u. with the chirality [indicated schematically in the inset of Fig. 4(b)] determined by the direction of **P**. Our calculations thus directly validate the previously proposed electric control of both the strength and chirality of DMI [see Fig. 1(a)]. We also find that A [Fig. 4(c)] and K_u [Fig. 4(d)] generally show opposite electric field dependences, i.e., as ε sweeps from 0.40 to -0.40 V/Å, A almost decreases linearly from 172.70 to 117.90 meV Å^2/f.u., while K_u is enhanced from 0.19 to 0.25 meV/f.u. With the application of electric field, M_s changes less than 1% and remains to be about 2.40 μ_B/f.u. in our calculations.

Realization of skyrmions in 2D multiferroics. With all the magnetic parameters calculated, we can study the realization of skyrmions in a CrN monolayer. As we have mentioned before, the deduced κ is only 1.68 when $\varepsilon = 0$, which indicates the existence of an isolated metastable skyrmion. To confirm this point, we perform a micromagnetic simulation [30] by relaxing a trial skyrmion spin configuration on a CrN nanodisk. After the relaxation, we find that a metastable skyrmion (see Fig. 5) with a higher energy of 0.30 meV than the

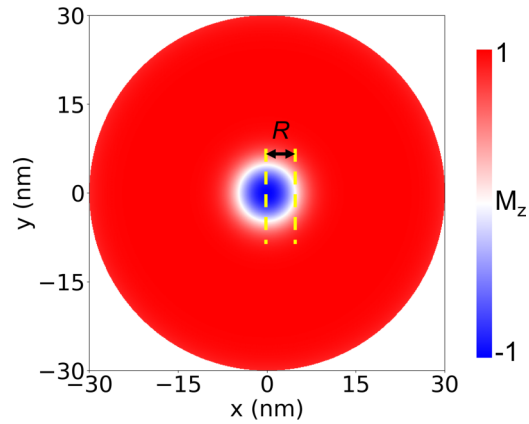

FIG. 5. The relaxed skyrmionic magnetization configuration in a CrN nanodisk with a radius of 30 nm in the absence of electric field. The out-of-plane component m_z is indicated by the color map. The radius R (defined as the radius of the $m_z = 0$ contour) of a relaxed skyrmion is 4.8 nm.

TABLE I. The calculated lattice constant a, film thickness t, saturation magnetization M_s, DMI parameter D, exchange stiffness A, magnetocrystalline anisotropy K_u, and dimensionless parameter κ for 2D multiferroics. The radius $\bar{R}$ of a skyrmion estimated by Eq. (3) is given for $CuVP_2Se_6$ and $CuCrP_2Se_6$. The sign of D is always determined for the structure with polarization oriented along the $+z$ direction.

Structure	a (Å)	t (nm)	M_s (μ_B/f.u.)	D (meV Å/f.u.)	A (meV Å^2/f.u.)	K_u (meV/f.u.)	κ	$\bar{R}$ (nm)
$CuVP_2S_6$	6.02	0.33	1.74	−0.07	90.96	−0.001	−310.23	
$CuVP_2Se_6$	6.38	0.33	1.75	1.70	44.70	0.15	3.46	1.2
$CuCrP_2S_6$	5.98	0.32	2.76	−0.47	119.64	−0.05	−66.85	
$CuCrP_2Se_6$	6.35	0.34	2.77	−2.50	111.96	0.17	4.18	1.6
Cr_8I_{23}	14.01	0.32	23.27	10.71	989.41	3.95	49.69	

ferromagnetic ground state can be stabilized. The radius R (defined as the radius of $m_z = 0$ contour) of a relaxed skyrmion is only 4.8 nm, which is very close to $\bar{R} = 4.5$ nm predicted by the theoretical formula [45]

$$\bar{R} = \pi D \sqrt{\frac{A}{16AK^2 - \pi^2 D^2 K}}. \quad (3)$$

For $|\varepsilon| < 0.50\,\mathrm{V/Å}$, κ varies between 1.44 and 2.67, and the relaxed radius R changes between 1.9 and 6.9 nm. Here, we should remind that along with the electric polarization switching, the chirality of the skyrmion is also switched as that of DMI. The four proposed interswitchable multiferrroic skyrmions with a tunable size [see Fig. 1(b)] can thus be realized in CrN monolayers.

To generalize the proposals for Rashba-type DMI and topological magnetism, we have considered other predicted 2D multiferroics including $CuMP_2X_6$ (M = Cr, V; X = S, Se) [22], and vacancy-doped CrI_3 (Cr_8I_{23}) [23]. Table I summarizes their calculated structural and magnetic parameters, which are also electrically switchable as for a CrN monolayer. From the calculation results, we can find that they all have a finite DMI, and the sizable D in $CuVP_2Se_6$ and $CuCrP_2Se_6$ can even lead to a relative small κ of ∼4.0, which is similar to those in Pd/Co/Pt ($\kappa = 5.4$) [33] and Fe/W(110) ($\kappa = 4.8$) [46] that are anticipated to host chiral magnetic solitons [33,47]. Considering that the predicted radius $\bar{R}$ of skyrmions in $CuVP_2Se_6$ and $CuCrP_2Se_6$ is only about twice their lattice constant a, the classical description of $E[q]$ in Eq. (1) may fail, and quantum effects should be taken into account [48], which deserves further study in the future.

Conclusion. We have performed first-principles calculations and micromagnetic simulations to demonstrate the existence of Rashba-type DMI and skyrmions in 2D multiferroics. Due to the intrinsic coupling of magnetism and electric polarization in 2D multiferroics, both the strength and chirality of the DMI, and thereby the size and chirality of the skyrmion, can be effectively controlled by electric field. A significant Rashba-type DMI may not only promote the stabilization of topological magnetism as already described in our work, but also enable the efficient current-induced motion of domain walls [49,50] as well as skyrmions [51] by spin-orbit torque (SOT), which is particularly important in practical applications. Although we have focused on 2D multiferroics with vertical polarization, our proposal for the electric control of DMI and topological magnetism can be easily extended to those with in-plane polarization [52–54], in which the DMI can be generated through other mechanisms rather than the Rashba effect. Recently, Xu *et al.* [55] discussed the manipulation of bimerons in VOI_2 monolayers with in-plane polarization. In summary, our work can open up a different route to the generation and electric control of topological magnetism in emerging 2D spintronics.

Acknowledgments. The authors thank Dr. Erjia Guo, Dr. Youguo Shi, Prof. Bin Xiang, Prof. Chunlei Gao, Prof. Mairbek Chshiev and Prof. Albert Fert for the fruitful discussions and collaborations on related topics. This work was supported by the National Natural Science Foundation of China (11874059), the Key Research Program of Frontier Sciences, CAS, Grant No. ZDBS-LY-7021, and Zhejiang Province Natural Science Foundation of China (LR19A040002).

[1] M. Bode, M. Heide, K. Von Bergmann, P. Ferriani, S. Heinze, G. Bihlmayer, A. Kubetzka, O. Pietzsch, S. Blügel, and R. Wiesendanger, Nature (London) **447**, 190 (2007).
[2] Y. Cao, Z. Huang, Y. Yin, H. Xie, B. Liu, W. Wang, C. Zhu, D. Mandrus, L. Wang, and W. Huang, Mater. Today Adv. **7**, 100080 (2020).
[3] A. N. Bogdanov and D. A. Yablonskii, Sov. Phys. JETP **68**, 101 (1989).
[4] S. Mühlbauer, B. Binz, F. Jonietz, C. Pfleiderer, A. Rosch, A. Neubauer, R. Georgii, and P. Böni, Science **323**, 915 (2009).
[5] X. Yu, Y. Onose, N. Kanazawa, J. Park, J. Han, Y. Matsui, N. Nagaosa, and Y. Tokura, Nature (London) **465**, 901 (2010).
[6] I. Dzyaloshinsky, J. Phys. Chem. Solids **4**, 241 (1958).
[7] T. Moriya, Phys. Rev. **120**, 91 (1960).
[8] S. Heinze, K. von Bergmann, M. Menze, J. Brede, A. Kubetzka, R. Wiesendanger, G. Bihlmayer, and S. Blugel, Nat. Phys. **7**, 713 (2011).
[9] N. Romming, C. Hanneken, M. Menzel, J. E. Bickel, B. Wolter, K. von Bergmann, A. Kubetzka, and R. Wiesendanger, Science **341**, 636 (2013).
[10] O. Boulle *et al.*, Nat. Nanotechnol. **11**, 449 (2016).
[11] C. Gong, L. Li, Z. Li, H. Ji, A. Stern, Y. Xia, T. Cao, W. Bao, C. Wang, Y. Wang, Z. Q. Qiu, R. J. Cava, S. G. Louie, J. Xia, and X. Zhang, Nature (London) **546**, 265 (2017).
[12] B. Huang, G. Clark, E. Navarro-Moratalla, D. R. Klein, R. Cheng, K. L. Seyler, D. Zhong, E. Schmidgall, M. A. McGuire, D. H. Cobden, W. Yao, D. Xiao, P. Jarillo-Herrero, and X. Xu, Nature (London) **546**, 270 (2017).

[13] M. Bonilla, S. Kolekar, Y. Ma, H. C. Diaz, V. Kalappattil, R. Das, T. Eggers, H. R. Gutierrez, M.-H. Phan, and M. Batzill, Nat. Nanotechnol. **13**, 289 (2018).
[14] D. J. O'Hara, T. Zhu, A. H. Trout, A. S. Ahmed, Y. K. Luo, C. H. Lee, M. R. Brenner, S. Rajan, J. A. Gupta, D. W. McComb, and R. K. Kawakami, Nano Lett. **18**, 3125 (2018).
[15] Y. Deng, Y. Yu, Y. Song, J. Zhang, N. Z. Wang, Z. Sun, Y. Yi, Y. Z. Wu, S. Wu, J. Zhu, J. Wang, X. H. Chen, and Y. Zhang, Nature (London) **563**, 94 (2018).
[16] J. H. Liang, W. W. Wang, H. F. Du, A. Hallal, K. Garcia, M. Chshiev, A. Fert, and H. X. Yang, Phys. Rev. B **101**, 184401 (2020).
[17] K.-W. Kim, H.-W. Lee, K.-J. Lee, and M. D. Stiles, Phys. Rev. Lett. **111**, 216601 (2013).
[18] A. Kundu and S. Zhang, Phys. Rev. B **92**, 094434 (2015).
[19] I. A. Ado, A. Qaiumzadeh, R. A. Duine, A. Brataas, and M. Titov, Phys. Rev. Lett. **121**, 086802 (2018).
[20] B. Dieny and M. Chshiev, Rev. Mod. Phys. **89**, 025008 (2017).
[21] W. Luo, K. Xu, and H. Xiang, Phys. Rev. B **96**, 235415 (2017).
[22] J. Qi, H. Wang, X. Chen, and X. Qian, Appl. Phys. Lett. **113**, 043102 (2018).
[23] Y. Zhao, L. Lin, Q. Zhou, Y. Li, S. Yuan, Q. Chen, S. Dong, and J. Wang, Nano Lett. **18**, 2943 (2018).
[24] S. Seki, X. Z. Yu, S. Ishiwata, and Y. Tokura, Science **336**, 198 (2012).
[25] Y. Okamura, F. Kagawa, S. Seki, and Y. Tokura, Nat. Commun. **7**, 12669 (2016).
[26] L. Wang, Q. Feng, Y. Kim, R. Kim, K. H. Lee, S. D. Pollard, Y. J. Shin, H. Zhou, W. Peng, D. Lee, W. Meng, H. Yang, J. H. Han, M. Kim, Q. Lu, and T. W. Noh, Nat. Mater. **17**, 1087 (2018).
[27] N. Nagaosa and Y. Tokura, Nat. Nanotechnol. **8**, 899 (2013).
[28] Y. Liu, S. J. Xuan, M. Jia, and H. Yan, J. Phys. D: Appl. Phys. **50**, 48LT01 (2017).
[29] V. M. Kuchkin and N. S. Kiselev, Phys. Rev. B **101**, 064408 (2020).
[30] See Supplemental Material at http://link.aps.org/supplemental/10.1103/PhysRevB.102.220409 for (1) descriptions of the qSO method to determine the magnetic parameters, and (2) details of first-principles calculations and micromagnetic simulations, which includes Refs. [34–39].
[31] S. Rohart and A. Thiaville, Phys. Rev. B **88**, 184422 (2013).
[32] A. O. Leonov, T. I. Monchesky, N. Romming, A. Kubetzka, A. N. Bogdanov, and R. Wiesendanger, New J. Phys. **18**, 065003 (2016).
[33] H. Jia, B. Zimmermann, and S. Blügel, Phys. Rev. B **98**, 144427 (2018).
[34] L. M. Sandratskii, Phys. Rev. B **96**, 024450 (2017).
[35] G. Kresse and J. Furthmüller, Phys. Rev. B **54**, 11169 (1996).
[36] M. Heide, G. Bihlmayer, and S. Blügel, Physica B (Amsterdam) **404**, 2678 (2009).
[37] J. P. Perdew, K. Burke, and M. Ernzerhof, Phys. Rev. Lett. **77**, 3865 (1996).
[38] M. J. Donahue and D. G. Porter, Interagency Report No. NISTIR 6376, National Institute of Standards and Technology, 1999, http://math.nist.gov/oommf/.
[39] T. L. Gilbert, Phys. Rev. **100**, 1243 (1955).
[40] A. V. Kuklin, A. A. Kuzubov, E. A. Kovaleva, N. S. Mikhaleva, F. N. Tomilin, H. Lee, and P. V. Avramov, Nanoscale **9**, 621 (2017).
[41] H. X. Yang, A. Thiaville, S. Rohart, A. Fert, and M. Chshiev, Phys. Rev. Lett. **115**, 267210 (2015).
[42] A. Belabbes, G. Bihlmayer, F. Bechstedt, S. Blügel, and A. Manchon, Phys. Rev. Lett. **117**, 247202 (2016).
[43] H. X. Yang, G. Chen, A. A. C. Cotta, A. T. N'Diaye, S. A. Nikolaev, E. A. Soares, W. A. A. Macedo, K. Liu, A. K. Schmid, A. Fert, and M. Chshiev, Nat. Mater. **17**, 605 (2018).
[44] For the convenience of comparison with future experiments, we also present the converted values of magnetic parameters when the unit of E[q] is changed from meV/f.u. to J/m^3, as indicated by the blue right axes in Figs. 4(b)–4(d). It is difficult to define the thickness of the CrN monolayer, and here we take it to be $t = 0.2$ nm as for the Co monolayer [B. Zimmermann, G. Bihlmayer, M. Böttcher, M. Bouhassoune, S. Lounis, J. Sinova, S. Heinze, S. Blügel, and B. Dupé, Phys. Rev. B **99**, 214426 (2019)].
[45] X. S. Wang, H. Y. Yuan, and X. R. Wang, Commun. Phys. **1**, 31 (2018).
[46] M. Heide, G. Bihlmayer, and S. Blügel, Phys. Rev. B **78**, 140403(R) (2008).
[47] M. Hoffmann, B. Zimmermann, G. P. Müller, D. Schürhoff, N. S. Kiselev, C. Melcher, and S. Blügel, Nat. Commun. **8**, 308 (2017).
[48] O. M. Sotnikov, V. V. Mazurenko, J. Colbois, F. Mila, M. I. Katsnelson, and E. A. Stepanov, arXiv:2004.13526.
[49] A. Thiaville, S. Rohart, E. Jue, V. Cros, and A. Fert, Europhys. Lett. **100**, 57002 (2012).
[50] I. Smaili, S. Laref, J. H. Garcia, U. Schwingenschlogl, S. Roche, and A. Manchon, arXiv:2007.07579.
[51] S. Woo, K. M. Song, H.-S. Han, M.-S. Jung, M.-Y. Im, K.-S. Lee, K. S. Song, P. Fischer, J.-I. Hong, J. W. Choi, B.-C. Min, H. C. Koo, and J. Chang, Nat. Commun. **8**, 15573 (2017).
[52] C. X. Huang, Y. P. Du, H. P. Wu, H. J. Xiang, K. M. Deng, and E. J. Kan, Phys. Rev. Lett. **120**, 147601 (2018).
[53] H. X. Tan, M. L. Li, H. T. Liu, Z. R. Liu, Y. C. Li, and W. H. Duan, Phys. Rev. B **99**, 195434 (2019).
[54] M. L. Xu, C. X. Huang, Y. W. Li, S. Y. Liu, X. Zhong, P. Jena, E. J. Kan, and Y. C. Wang, Phys. Rev. Lett. **124**, 067602 (2020).
[55] C. S. Xu, P. Chen, H. X. Tan, Y. R. Yang, H. J. Xiang, and L. Bellaiche, Phys. Rev. Lett. **125**, 037203 (2020).